

---

# CUDA-GR: Controllable Unsupervised Domain Adaptation for Gaze Redirection

---

Swati Jindal, Xin Eric Wang

Department of Computer Science and Engineering  
UC Santa Cruz

{swjindal, xwang366}@ucsc.edu

## Abstract

The aim of gaze redirection is to manipulate the gaze in an image to the desired direction. However, existing methods are inadequate in generating perceptually reasonable images. Advancement in generative adversarial networks has shown excellent results in generating photo-realistic images. Though, they still lack the ability to provide finer control over different image attributes. To enable such fine-tuned control, one needs to obtain ground truth annotations for the training data which can be very expensive. In this paper, we propose an unsupervised domain adaptation framework, called CUDA-GR, that learns to disentangle gaze representations from the labeled source domain and transfers them to an unlabeled target domain. Our method enables fine-grained control over gaze directions while preserving the appearance information of the person. We show that the generated image-labels pairs in the target domain are effective in knowledge transfer and can boost the performance of the downstream tasks. Extensive experiments on the benchmarking datasets show that the proposed method can outperform state-of-the-art techniques in both quantitative and qualitative evaluation.

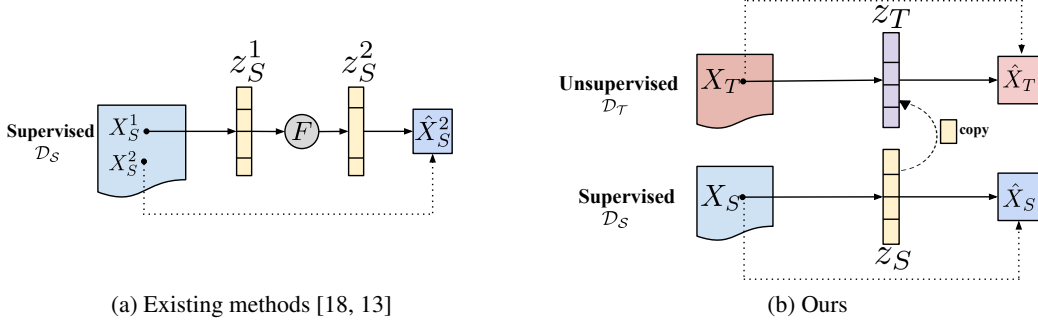
## 1 Introduction

Gaze behavior plays a pivotal role in the analysis of non-verbal cues and can provide support to various applications such as virtual reality [1, 2], human-computer interaction [3, 4], cognition [5, 6], and social sciences [7, 8]. A robust gaze representation learning requires a large amount of training data which is time-consuming and expensive to manually collect, especially when labels are continuous. Although many methods [9–11] have been proposed to tackle the data need, they fail to generalize well to in-the-wild images.

Various gaze redirection methods [12–14] have been explored as an alternate solution for generating more labeled training data using generative adversarial networks (GANs) [15] based frameworks. However, these methods require paired images for learning image-to-image translations and thus cannot generalize faithfully to new domain images. Furthermore, enabling finer control to manipulate certain image attributes through generative models remains challenging due to the entanglement of different factors of variations during the generation process, and this limits their application in providing accurate supervised data beneficial for certain downstream tasks. Recent works [16, 17] learn the manipulation of individual visual attributes in the real scene, however, they assume the availability of simulated data with pre-defined labeled attributes which might not be easily accessible for the task at hand.

In this work, we propose an unsupervised domain adaptation framework in the cross-domain setting which provides explicit control of eye gaze and head pose directions to manipulate images without any need for labeled data in the target domain. To render such kind of control, our method learns the disentangled representations for explicit factors, like gaze and head orientations, along with

Figure 1: **Comparison of existing methods vs. Ours:** Here,  $\mathcal{D}_S$  and  $\mathcal{D}_T$  represent source and target domains. (a) Previous approaches [18, 13] assumes the paired image-to-image translation ( $X_S^1 \rightarrow X_S^2$ ) learning for a single domain  $\mathcal{D}_S$  and uses a transforming function  $F$  in the latent space to ensure disentanglement. (b) Our method auto-encodes the images  $X_S, X_T$  from two domains  $\mathcal{D}_S, \mathcal{D}_T$ , respectively into a common disentangled space using labels only from  $\mathcal{D}_S$ , and transfers latent factors during inference via a simple copy operation.



implicit factors such as appearance, illumination, shadows, etc. from a labeled source domain. This learned disentangling behavior can be duplicated for the target domain images, and thus enables the manipulation over explicit factors, while simultaneously maintaining the implicit factors.

Previous approaches [18, 13] learn the control over multiple variation factors and make use of supervised paired samples for training. In contrast, our method assimilates this behavior without any input-output paired samples and in an unsupervised setting, since only unlabeled data is available in the target domain during the training stage. We exploit the auto-encoding property to map the source and target domain data into a single disentangled latent space which allows the transfer of explicit latent factors from source to target domain images. Thus, the proposed method can be adapted to multiple domain datasets, and hence, it is more generalizable. The overview of differences of our method with the previous approaches is shown in Figure 1. In addition, our method can be used to generate images with out-of-distribution labels. To the best of our knowledge, we are first to address the problem of gaze redirection in an unsupervised cross-domain adaptation setting.

We train our model on GazeCapture [19] and demonstrate the effectiveness of the proposed method on two target domain datasets: MPIIGaze [20] and Columbia [21], achieving better results than state-of-the-art methods [18, 13] in terms of both qualitative and quantitative evaluation. Our method shows high quality in preserving the photo-realism and faithfully rendering the desired gaze direction. Additionally, our framework also shows promising results on the performance of the gaze estimation task. In this work,

1. we propose an end-to-end learning framework for unsupervised domain adaptation for transferring the disentangled latent knowledge from the labeled source domain to the unlabeled target domain.
2. our method enables fine-grained control over gaze directions and exhibits the superior quality of the generated images while preserving the person-specific appearance factors.
3. we provide the application of the proposed method for improving the downstream task performance on gaze estimation.

## 2 Related Work

**Gaze redirection** The end-to-end gaze estimation learning based methods require a large amount of labeled data to handle variations in appearances and different head poses. To tackle the need of such a volume of data, multiple works have focused on the task of redirecting gaze to attain more data for the gaze estimation task. Kononenko et al. [22] use random forests as their supervised learning method to predict flow field for gaze correction. Various works [23–25] employ a deep neural network to learn the warping flow field between images along with a correction term, however, these warping-based methods cannot generalize well to the large gaze and head pose directions. He et al. [26] proposes a

GAN-based framework with a cycle consistency loss to learn gaze redirection and can generate images with high resolution, however, it cannot generalize well to the images taken in a real-world setting. Wood et. al [27] use a graphic pipeline to redirect eye images by fitting morphable models, however, modeling-based methods make assumptions that do not hold in practice. Mask-based generator networks [28] have also been explored for the task of gaze redirection, though their performance is highly dependent on the accuracy of the segmentation module [12]. Park et. al [18] uses a transforming encoder-decoder based network [29, 30] to learn disentanglement in the latent space, although their method cannot generate photo-realistic redirected images. Recently, [14, 13] proposes controllable gaze redirection methods which allow controlling the gaze explicitly, nonetheless, they make use of paired training samples for learning the task of gaze redirection, while in contrast, our method does not require any paired input-output samples and can be adapted to any target domain without the need of labels.

**Representation disentanglement** The goal of learning disentangled representations is to model the factors of data variations. Various methods [31–34] have been explored in a supervised setting. These methods exploit the semantic knowledge gained from the available annotations to learn the factorized representations. On the other hand, unsupervised disentanglement methods [35–37] learn the same behavior but without requiring any labeled data. However, these methods provide limited flexibility to select a specific factor of variation and are focused on manipulating the data in a single domain. Unsupervised cross-domain disentanglement methods [38, 39] present a framework that takes advantage of domain shared and domain specific attributes to provide a manipulation tool based on the appearance and content of the image. Synthetic data is used by few works [16, 17] to control various aspects and thus, assumes the availability of rendered data through a graphics pipeline with pre-defined labeled attributes. Liu et al. [40] is designed to provide control over the labeled factors using the images from two domains and is trained in a semi-supervised setting but their work is applicable only on categorical labels. In this work, we specifically focus on manipulating continuous-valued labels in the cross-domain setting.

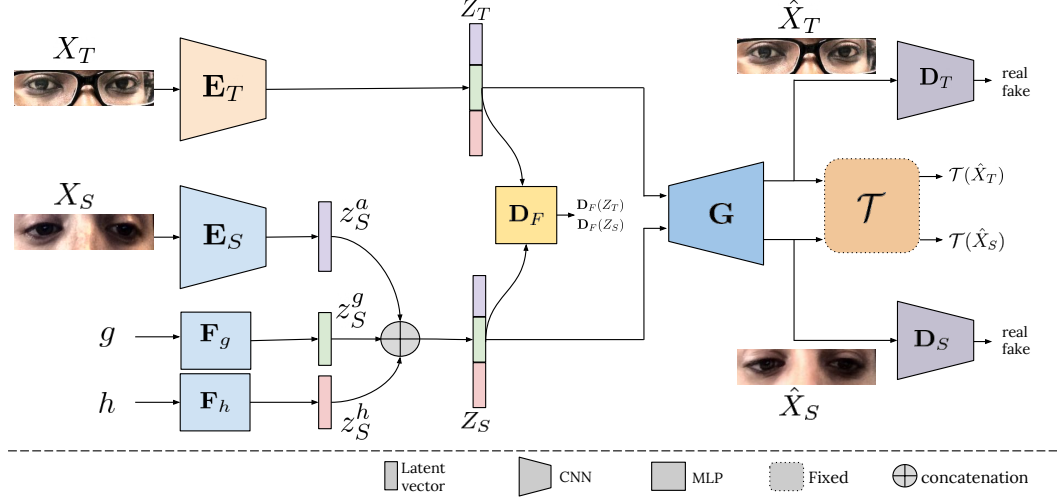
### 3 Proposed Method

The main idea behind our method is to disentangle the latent space so that each factor of variation can be controlled separately. Thus, our goal is to learn a network  $\mathbf{C}$  such that given an input image  $X_T$  and subset of explicit factors  $\{e_i\}$ , in our case gaze and head pose directions, it generates the image  $X_O$  satisfying the attributes described by  $\{e_i\}$  i.e.,  $C : (X_T, e_i) \rightarrow X_O$ . Unlike previous works [14, 13] that utilize input-output image pairs assuming that  $X_O$  is available during training, our method does not require any already available image pairs during training or inference time. We train our network on the labeled source domain and simultaneously adapt it to the unlabeled target domain. We call our framework CUDA-GR. We start with the assumption that there are three factors of variations: 1) appearance-based factors, including illumination, shadows, personal varying factors, etc., which might or might not be explicitly labeled with the dataset, 2) eye gaze direction and 3) head pose angles. We have gaze and head pose labels available only for the source domain data. Thus, using the supervision from source data, we learn the disentanglement for these three factors of variations in the latent space and transfer the learned behavior to the unsupervised target domain data. Following the notations used in [18], we represent the appearance-related latent factor as  $z^a$ , gaze latent factor  $z^g$ , and head pose latent factor  $z^h$ .

#### 3.1 Model

The overall architecture of CUDA-GR is shown in the Figure 2. The bottom part of the network consists of a source encoder  $\mathbf{E}_S$  which encodes a source domain image  $X_S$  to  $z_S^a$ . We assume that  $\mathbf{E}_S$  only encodes the appearance-related information from the images, which is not already available beforehand. The latent  $z_S^g$  and  $z_S^h$  are learned separately through 2 separate MLP-based blocks  $\mathbf{F}_g$  and  $\mathbf{F}_h$  which take the gaze  $g$  and head pose  $h$  corresponding to image  $X_S$  as inputs, respectively. Thus, the overall embedding  $Z_S$  related to image  $X_S$  can be formed by combining the information from three factors of variations, i.e.  $Z_S = z_S^a \oplus z_S^g \oplus z_S^h$  (here  $\oplus$  denotes concatenation). Further,  $Z_S$  is passed through a generator network  $\mathbf{G}$  which decodes it to the output image given by  $\hat{X}_S$  and is trained in an adversarial manner with the discriminator network  $\mathbf{D}_S$ . The upper part of the network constitutes an auto-encoder based architecture with an encoder  $\mathbf{E}_T$ .  $\mathbf{E}_T$  takes an image  $X_T$  from

Figure 2: **Overview of the CUDA-GR architecture.** The framework consists of domain specific encoders:  $E_T$  encode the target domain image  $X_T$  to  $Z_T$ , and  $\{E_S, F_g, F_h\}$  encode the source domain image  $X_S$ , gaze  $g$  and head pose  $h$  to  $z_S^a$ ,  $z_S^g$  and  $z_S^h$ , respectively. Then,  $z_S^a$ ,  $z_S^g$  and  $z_S^h$  are concatenated to form overall embedding  $Z_S$  for the source domain image  $X_S$ . These domain specific encoded embeddings  $Z_T$  and  $Z_S$  are passed through a shared generator network  $G$ , and also through a latent domain discriminator network  $D_F$ .  $D_T$  and  $D_S$  represents two domain specific image discriminator networks and  $\mathcal{T}$  is the pre-trained task network which is fixed during training. The whole framework is learnt in an end-to-end manner. Please refer to Section 3 for more details.



the unlabeled target domain data and outputs an embedding  $Z_T$ . We consider  $Z_T$  to be semantically equivalent to  $Z_S$ , i.e.,  $Z_T$  implicitly embeds the information related to all three factors of variations (appearance, gaze, and head pose). Note that the dimension of  $Z_T$  and  $Z_S$  are same, thus  $Z_T$  can be divided into  $\{z_T^a, z_T^g, z_T^h\}$ . The embedding  $Z_T$  is then passed through the shared generator  $G$  and outputs  $\hat{X}_T$ , which is trained in an adversarial manner with the discriminator network  $D_T$ .

During the inference, for controlling gaze and head pose directions of the target image, we pass the image  $X_T$  through the encoder  $E_T$ , desired gaze  $g$ , and head pose  $h$  through  $F_g$  and  $F_h$  giving us  $Z_T$ ,  $z_S^g$  and  $z_S^h$ , respectively. Recall that  $Z_T$  constitutes of  $\{z_T^a, z_T^g, z_T^h\}$ , thus replacing  $\{z_T^g, z_T^h\}$  with  $\{z_S^g, z_S^h\}$  will form the embedding satisfying the target conditions and can be passed through the generator  $G$  to output image  $\hat{X}_T^{g,h}$  with gaze  $g$  and head pose  $h$ , i.e.,

$$\hat{X}_T^{g,h} = G(z_T^a \oplus z_S^g \oplus z_S^h) \quad (1)$$

Likewise, we can also control the individual factor of gaze (or head pose) by replacing only  $z_T^g$  (or  $z_T^h$ ) with  $z_S^g$  (or  $z_S^h$ ), such that  $\hat{X}_T^g = G(z_T^a \oplus z_S^g \oplus z_T^h)$  and  $\hat{X}_T^h = G(z_T^a \oplus z_T^g \oplus z_S^h)$ .

### 3.2 Learning Objectives

The overall objective of our method is to learn a common disentangled latent space for both source and target domain such that the individual latent factors can be easily transferred to manipulate target images. To ensure this, we train our framework using multiple objective functions each of which are explained in detail below.

**Reconstruction Loss:** We apply pixel-wise L1 reconstruction loss between the generated image  $\hat{X}_{\{T,S\}}$  and input image  $X_{\{T,S\}}$  to ensure the auto-encoding behavior.

$$\mathcal{L}_R(\hat{X}, X) = \frac{1}{|X|} \|\hat{X} - X\|_1 \quad (2)$$

Thus, the total reconstructions loss is defined as:

$$\mathcal{L}_{recon} = \mathcal{L}_{\mathcal{R}}(\hat{X}_T, X_T) + \mathcal{L}_{\mathcal{R}}(\hat{X}_S, X_S) \quad (3)$$

**Perceptual Loss:** To ensure that our generated images perceptually matches the input images, we apply the perceptual loss [41] which is defined as a mean-square loss between the activations of a pre-trained neural network applied between the generated image  $\hat{X}_{\{T,S\}}$  and input image  $X_{\{T,S\}}$ . For this, we use VGG-16 [42] network trained on ImageNet [43].

$$\mathcal{L}_{\mathcal{P}}(\hat{X}, X) = \sum_{i=1}^4 \frac{1}{|\psi_i(X)|} \|\psi_i(\hat{X}) - \psi_i(X)\|_2 \quad (4)$$

where  $\psi$  denotes VGG-16 network. Therefore, our overall perceptual loss becomes:

$$\mathcal{L}_{perc} = \mathcal{L}_{\mathcal{P}}(\hat{X}_T, X_T) + \mathcal{L}_{\mathcal{P}}(\hat{X}_S, X_S) \quad (5)$$

**Consistency Loss:** To preserve the gaze and head pose information, we apply a consistency loss between the generated image  $\hat{X}_{\{T,S\}}$  and input image  $X_{\{T,S\}}$ . For this, we use a pre-trained task network  $\mathcal{T}$  which predicts the pseudo-labels (gaze and head pose) for an image. It consists of two terms: (a) *label consistency loss* ensures the consistency between pseudo-labels for input and the generated images, and (b) *redirection consistency loss* guarantees to preserve the pseudo-labels for redirected images. For the second term, we generate gaze redirected images in the target domain as  $\hat{X}_T^g = \mathbf{G}(z_T^a \oplus z_S^g \oplus z_T^h)$ , and head redirected images as  $\hat{X}_T^h = \mathbf{G}(z_T^a \oplus z_T^g \oplus z_S^h)$ . We enforce the consistency of gaze and head pose predictions for  $\hat{X}_T^g$  with the pseudo gaze label for  $X_S$  and pseudo head pose label for  $\hat{X}_T$ , i.e.,  $\mathcal{T}^g(\hat{X}_T^g) = \mathcal{T}^g(X_S)$  and  $\mathcal{T}^h(\hat{X}_T^g) = \mathcal{T}^h(X_T)$ . A similar argument holds for the head redirected image  $\hat{X}_T^h$ . Here,  $\mathcal{T}^g$  and  $\mathcal{T}^h$  represent the gaze and head pose predicting layers of  $\mathcal{T}$ .

The overall gaze consistency loss will become

$$\begin{aligned} \mathcal{L}_{gaze} = & \underbrace{\mathcal{L}_{ang}(\mathcal{T}^g(\hat{X}_S), \mathcal{T}^g(X_S)) + \mathcal{L}_{ang}(\mathcal{T}^g(\hat{X}_T), \mathcal{T}^g(X_T))}_{\text{label consistency loss}} \\ & + \underbrace{\mathcal{L}_{ang}(\mathcal{T}^g(\hat{X}_T^g), \mathcal{T}^g(X_S)) + \mathcal{L}_{ang}(\mathcal{T}^g(\hat{X}_T^h), \mathcal{T}^g(X_T))}_{\text{redirection consistency loss}} \end{aligned} \quad (6)$$

where,

$$\mathcal{L}_{ang}(\hat{\mathbf{u}}, \mathbf{u}) = \arccos \left( \frac{\hat{\mathbf{u}} \cdot \mathbf{u}}{\|\hat{\mathbf{u}}\| \cdot \|\mathbf{u}\|} \right) \quad (7)$$

Similarly, we can compute the head pose consistency loss  $\mathcal{L}_{head}$  (Appendix B). Hence, total consistency loss is defined as

$$\mathcal{L}_{consistency} = \mathcal{L}_{gaze} + \mathcal{L}_{head} \quad (8)$$

**GAN Loss:** To enforce photo-realistic output from the generator  $\mathbf{G}$ , we apply the standard GAN loss [15] to both image discriminators  $\mathbf{D}_S$  and  $\mathbf{D}_T$ .

$$\begin{aligned} \mathcal{L}_{GAN_D}(D, X, \hat{X}) &= \log D(X) + \log(1 - D(\hat{X})) \\ \mathcal{L}_{GAN_G}(D, \hat{X}) &= \log D(\hat{X}) \end{aligned} \quad (9)$$

The final GAN loss is defined as:

$$\begin{aligned} \mathcal{L}_{disc} &= \mathcal{L}_{GAN_D}(\mathbf{D}_T, X_T, \hat{X}_T) + \mathcal{L}_{GAN_D}(\mathbf{D}_S, X_S, \hat{X}_S) \\ \mathcal{L}_{gen} &= \mathcal{L}_{GAN_G}(\mathbf{D}_T, \hat{X}_T) + \mathcal{L}_{GAN_G}(\mathbf{D}_S, \hat{X}_S) \end{aligned} \quad (10)$$

**Domain Adversarial Loss:** We employ a latent domain discriminator network  $\mathbf{D}_F$  and train it using the following domain adversarial loss [44] to push the distribution of  $Z_T$  closer to  $Z_S$ .

$$\mathcal{L}_{feat}(\mathbf{D}_F, Z_T, Z_S) = \log \mathbf{D}_F(Z_S) + \log(1 - \mathbf{D}_F(Z_T)) \quad (11)$$

**Overall Objective:** Altogether, our final loss function for training encoders and generator network is

$$\mathcal{L}_{overall} = \lambda_R \mathcal{L}_{recon} + \lambda_P \mathcal{L}_{perc} + \lambda_C \mathcal{L}_{consistency} + \lambda_G \mathcal{L}_{gen} + \lambda_F \mathcal{L}_{feat} \quad (12)$$

## 4 Experiments

### 4.1 Datasets

**GazeCapture** [19] is the largest publicly available gaze dataset consisting of around 2M frames taken from unique 1474 subjects. Following the split defined in [19], we use data from 1274 subjects for training, 50 for validation, and 150 for test.

**MPIIGaze**<sup>1</sup> [20] is the most challenging dataset for the in-the-wild gaze estimation and includes higher within-subject variations in appearance, for example, illumination, make-up, and facial hair. We use the images from the standard evaluation subset MPIIFaceGaze [45] provided by MPIIGaze containing 37667 images captured from 15 subjects.

**Columbia** [21] contains 5880 high-resolution images from 56 subjects and displays larger diversity within participants. The images are collected in a constrained laboratory setting, with limited variations of head pose and gaze directions.

### 4.2 Implementation Details

The architecture of the encoders  $\mathbf{E}_S$ ,  $\mathbf{E}_T$ , and the generator network  $\mathbf{G}$  are DenseNet-based blocks as used in [18]. The gaze and head pose encoders  $\mathbf{F}_g$  and  $\mathbf{F}_h$ , each consists of 4 MLP layers with hidden dimensions equal to the input dimension. The task network  $\mathcal{T}$  is a ResNet-50 [46] based model trained on GazeCapture [19] training subset and gives 4-dimensional output, two angles for each gaze and head direction. The two image discriminators  $\mathbf{D}_S$  and  $\mathbf{D}_T$  share a similar PatchGAN [47] based architecture. The domain discriminator  $\mathbf{D}_F$  consists of 4 MLP-based layers. Note that,  $\mathcal{T}$  remains fixed during training of our whole pipeline.

All the datasets are pre-processed by a data normalization algorithm as described in [48]. Our input is a single image containing both eyes and has a size of  $64 \times 256$ . We use a data processing pipeline as employed in [18] to extract the eye image strip. The inputs gaze  $g$  and head pose  $h$  are two-dimensional pitch and yaw angles. The GazeCapture training subset is used as a labeled source domain while MPIIGaze and Columbia constitute as unlabeled target domains. Note that, we do not use any kind of labels from the target domain datasets while training our framework. More training details can be found in Appendix A.

### 4.3 Evaluation Metrics

We quantitatively measure the quality of generated images by computing Frechet Inception Distance (FID) [49] and Learned Perceptual Image Patch Similarity (LPIPS) [50]. FID [49] computes the distance between feature vectors obtained from InceptionNet [51] for generated samples and real samples. LPIPS [50] is used to measure the image pairwise similarity by calculating the distance in AlexNet [52] feature space. For measuring LPIPS, we assume the availability of paired samples along with the labels in the evaluation datasets. Finally, we show the applicability of the generated images in improving the performance on the downstream gaze estimation task.

### 4.4 Comparison to state-of-the-art

We adopt FAZE [18] and ST-ED [13] as our baseline methods. Both FAZE and ST-ED are based on transforming encoder-decoder architecture [29, 30] and apply known differences in gaze and head rotations to the embedding space for translating the input image to a redirected output image. FAZE [18] learns to control only explicit factors (gaze and head pose orientations) while ST-ED [13] allows controlling implicit factors too. Both of these methods assume the availability of paired data coming from a single source domain during training, while our method is trained in an unsupervised cross-domain setting without requiring any paired samples.

<sup>1</sup>This dataset is licensed under a CC BY-NC-SA 4.0 license.

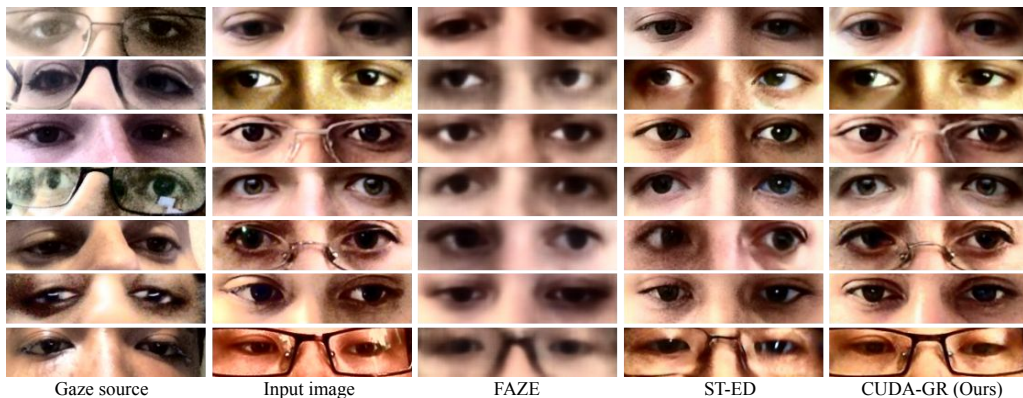
Table 1: **Quantitative evaluation:** Comparison with the baselines in terms of LPIPS and FID metrics (lower is better). Our framework CUDA-GR generates images that are perceptually closer to the ground-truth images, even though we do not use paired data samples while training.

	GazeCapture $\rightarrow$ MPIIGaze		GazeCapture $\rightarrow$ Columbia	
Method	LPIPS $\downarrow$	FID $\downarrow$	LPIPS $\downarrow$	FID $\downarrow$
FAZE [18]	0.369	108.4	0.477	238.2
ST-ED [13]	0.307	105.6	0.312	227.5
CUDA-GR (Ours)	<b>0.266</b>	<b>102.1</b>	<b>0.292</b>	<b>107.8</b>

FAZE [18] takes input as an image containing both eyes which is the same as in our method, thus necessary to compare to. We use original implementation<sup>2</sup> and trained models provided by the FAZE authors for comparison. In addition, we train ST-ED [13] network on images containing both eyes using the available public implementation<sup>3</sup> for a fair comparison with our method. Note that for ST-ED baseline, we compare only by altering explicit factors. For more details, please refer to Appendix A.3.3.

**Quantitative evaluation** Table 1 summarizes the quantitative evaluation of our method compared to the baselines. We evaluate the model in two settings: GazeCapture  $\rightarrow$  MPIIGaze which represents when the model is trained with source domain data as GazeCapture and target domain as MPIIGaze. Similarly, in GazeCapture  $\rightarrow$  Columbia, the target domain is Columbia. Note that, we compute FID between gaze redirected images and the ground-truth images while LPIPS is measure after redirecting both gaze and head pose. Our method outperforms the baseline methods by a large margin in terms of both LPIPS and FID metrics and shows consistent improvement in both target domains. We see a relative improvement in LPIPS of around 13.3% for the MPIIGaze dataset and 6.4% for the Columbia dataset. This shows that our method is more generalizable to different domain datasets and can be adapted to new datasets without the requirement of labels.

Figure 3: **Qualitative evaluation:** Comparison of the generated images from CUDA-GR (GazeCapture  $\rightarrow$  MPIIGaze) with the baseline methods FAZE [18] and ST-ED [13]. The first column shows the gaze source images from which gaze information is used to redirect. The second column shows the input images from the target domain data. Our method (column 5) produces better quality and photo-realistic images as compared to baseline methods (column 2 and 3). Best viewed in color.



**Qualitative evaluation** We also report the qualitative comparison of generated images in Figure 3 using a model trained with GazeCapture  $\rightarrow$  MPIIGaze. The results are shown on MPIIGaze dataset images which is the target domain dataset in this setting. As can be seen, our method produces

<sup>2</sup>[https://github.com/NVlabs/few\\_shot\\_gaze](https://github.com/NVlabs/few_shot_gaze)

<sup>3</sup><https://github.com/zhengyuf/STED-gaze>



Table 2: **Comparison to fully supervised baseline:** We compare our model with the ST-ED baseline trained in a fully supervised manner on the MPIIGaze data. Impressively, our model shows comparable performance to the fully supervised baseline model while being trained with zero supervision (from target domain) and no paired samples. It is worth noting that the inception score (FID) for our method is even better than ST-ED baseline, implying high quality of generated images.

	LPIPS↓	FID↓
ST-ED [13]	<b>0.264</b>	99.7
CUDA-GR (Ours)	0.273	<b>82.1</b>

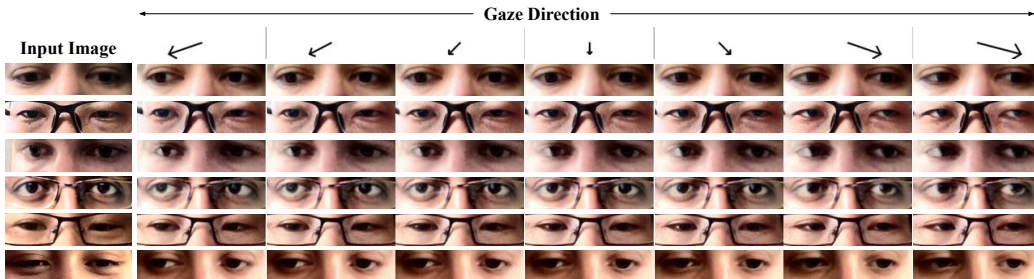
more photo-realistic images while preserving the appearance information and faithfully reproducing the gaze direction, when compared with FAZE [18] and ST-ED [13]. It is also worth noting that our method generates high-quality images for people with glasses (rows 3, 5, 7 in Figure 3) and also maintains the eye color (row 4 in Figure 3). These results are consistent with our findings in quantitative evaluation. More qualitative results are provided in Appendix D.

**Comparison to fully supervised baseline** We also compare our model with the ST-ED baseline trained on the MPIIGaze dataset in a fully supervised setting, i.e., using paired input-output samples from the MPIIGaze dataset along with the labels. For this experiment, we train both ST-ED [13] and our model on 11 users data from MPIIGaze and reserve 4 people data for evaluation. We compare both methods by measuring the LPIPS metric on the evaluation subset. Here, we expect that the ST-ED model will provide a lower bound for the evaluation metric as it is trained on the target domain dataset in a fully supervised setting. The results for this experiment are shown in Table 2. Our method shows a better FID score than the ST-ED baseline, thus indicating the better quality of generated images. Also, it can be seen that the LPIPS score is closer to the ST-ED model trained in a fully supervised setting while our method learns without any paired supervision and labels from the target domain.

#### 4.5 Controllable Gaze Redirection

Figure 4 shows the effectiveness of our method in controlling the gaze direction for various appearances. Our network takes the image (shown in Column 1, Figure 4) and desired gaze consisting of pitch and yaw angles (shown in Row 1, Figure 4) as inputs. Then, we replace the gaze latent factor corresponding to the original input image with the desired gaze latent feature to generate the redirected image (remaining columns and rows in Figure 4). We can see that our method faithfully renders the desired gaze while maintaining the appearance attributes of the image.

Figure 4: Effectiveness in redirecting images in the desired gaze direction in Row 1. Column 1 are the input images and the remaining are the redirected gaze images generated by CUDA-GR. Best viewed in color.

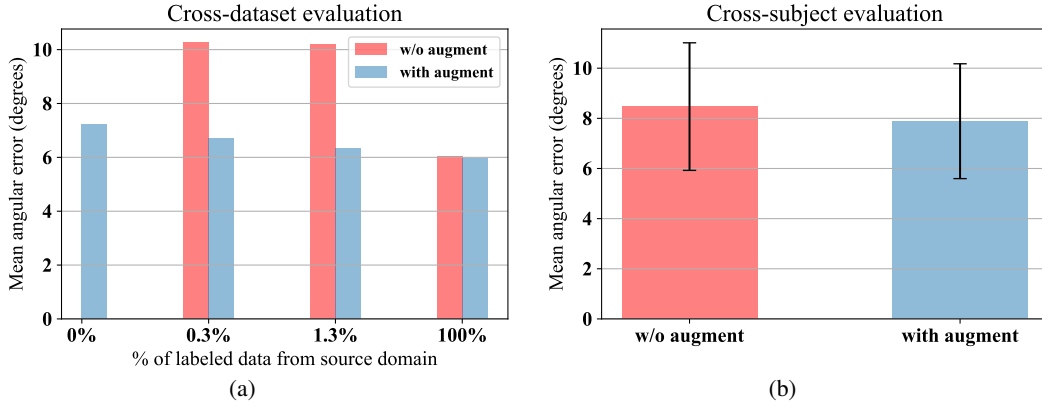


#### 4.6 Evaluation of Gaze Estimation Task

We also demonstrate the applicability of our method in improving the performance of the downstream gaze estimation task. For this, we conduct experiments for both cross-subject and cross-dataset



Figure 5: Comparison of cross-dataset and cross-subject gaze estimation task performance *with* or *without* augmented data. The addition of augmented data in the training set improves the overall accuracy (i.e., reduces the mean angular error) and is consistent for both experiments. Best viewed in color.



estimation and train a ResNet-50 [46] initialized with ImageNet pre-trained weights. Note that, this gaze estimation model is different from  $\mathcal{T}$  in our previous experiments, and is trained from scratch. Further, using our trained generator model, we create an augmented dataset ( $\sim 1\text{M}$  samples) by redirecting the MPIIGaze images using the explicit gaze direction sampled from the labeled source domain dataset.

In cross-dataset experiment, we assume the availability of few samples ( $= 9$ ) per person as the validation subset to choose the best performing model while the remaining samples are kept for testing. We train the gaze estimator model on GazeCapture training subset. Here, we conduct experiments in 4 different settings where we use  $x\%$  of labeled data from the source domain ( $x \in \{0, 0.3, 1.3, 100\}$ ), *with* and *without* adding the augmented dataset for training. For 0% labeled data, we train the model only using the augmented dataset. Figure 5 (a) shows the performance comparison and it can be seen that the addition of augmented data reduces the mean angular error for each setting of our evaluation, thus the augmented dataset help in ameliorating the gaze estimation performance.

For cross-subject evaluation, we adopt a leave-one-person out strategy and train our model on MPIIGaze [20] dataset. Figure 5 (b) shows the error bar plots for mean angular error (with standard deviation) computed for *with* and *without* augmented data. Again, we see a decrease in the mean angular error, which is consistent with our previous findings.

## 5 Conclusion

We present a domain adaptation framework trained in an unsupervised manner using cross-domain datasets for gaze redirection task. The proposed method takes advantage of both supervised source domain and unsupervised target domain to learn the disentangled factors of variation. Experimental results demonstrate the effectiveness of our model in generating photo-realistic images on multiple domain datasets while truly adapting the desired gaze direction. Due to no requirement of supervision in the target domain, our method can be easily extended to new datasets.

## Broader Impact

Our work presents a new setting for gaze redirection designed using an unsupervised cross-domain adaptation framework. Because of removing the requirement of annotations in the target domain, the applicability of our work increases for new datasets where manual annotations are hard to collect. Our method is relevant to various applications such as video conferencing, photo correction, and movie editing for redirecting gaze to establish eye contact with the viewer. It can also be extended to augment existing datasets for downstream tasks. As for any method enabling the photo-realistic image generation, malicious use is possible and thus could support deepfakes. However, our method does not handle extreme gaze directions due to the limitations of label distributions in public gaze datasets, which remains an open challenge, and it does not faithfully redirect the head pose. We encourage research community to consider societal impacts while improving such methods.

## References

- [1] A. Patney, J. Kim, M. Salvi, A. Kaplanyan, C. Wyman, N. Benty, A. Lefohn, and D. Luebke, “Perceptually-based foveated virtual reality,” in *ACM SIGGRAPH 2016 Emerging Technologies*, pp. 1–2, 2016.
- [2] T. Pfeiffer, “Towards gaze interaction in immersive virtual reality: Evaluation of a monocular eye tracking set-up,” in *Virtuelle und Erweiterte Realität-Fünfter Workshop der GI-Fachgruppe VR/AR*, 2008.
- [3] P. Majaranta and A. Bulling, “Eye tracking and eye-based human–computer interaction,” in *Advances in physiological computing*, pp. 39–65, Springer, 2014.
- [4] R. J. Jacob and K. S. Karn, “Eye tracking in human-computer interaction and usability research: Ready to deliver the promises,” in *The mind’s eye*, pp. 573–605, Elsevier, 2003.
- [5] G. T. Buswell, “How people look at pictures: a study of the psychology and perception in art,” 1935.
- [6] C. A. Rothkopf, D. H. Ballard, and M. M. Hayhoe, “Task and context determine where you look,” *Journal of vision*, vol. 7, no. 14, pp. 16–16, 2007.
- [7] R. Ishii, K. Otsuka, S. Kumano, and J. Yamato, “Prediction of who will be the next speaker and when using gaze behavior in multiparty meetings,” *ACM Transactions on Interactive Intelligent Systems (THIS)*, vol. 6, no. 1, pp. 1–31, 2016.
- [8] C. Oertel, K. A. Funes Mora, J. Gustafson, and J.-M. Odobez, “Deciphering the silent participant: On the use of audio-visual cues for the classification of listener categories in group discussions,” in *Proceedings of the 2015 ACM on International Conference on Multimodal Interaction*, pp. 107–114, 2015.
- [9] E. Wood, T. Baltrušaitis, X. Zhang, Y. Sugano, P. Robinson, and A. Bulling, “Rendering of eyes for eye-shape registration and gaze estimation,” in *Proceedings of the IEEE International Conference on Computer Vision*, pp. 3756–3764, 2015.
- [10] E. Wood, T. Baltrušaitis, L.-P. Morency, P. Robinson, and A. Bulling, “Learning an appearance-based gaze estimator from one million synthesised images,” in *Proceedings of the Ninth Biennial ACM Symposium on Eye Tracking Research & Applications*, pp. 131–138, 2016.
- [11] A. Shrivastava, T. Pfister, O. Tuzel, J. Susskind, W. Wang, and R. Webb, “Learning from simulated and unsupervised images through adversarial training,” in *Proceedings of the IEEE conference on computer vision and pattern recognition*, pp. 2107–2116, 2017.
- [12] H. Kaur and R. Manduchi, “Subject guided eye image synthesis with application to gaze redirection,” in *Proceedings of the IEEE/CVF Winter Conference on Applications of Computer Vision*, pp. 11–20, 2021.
- [13] Y. Zheng, S. Park, X. Zhang, S. De Mello, and O. Hilliges, “Self-learning transformations for improving gaze and head redirection,” *arXiv preprint arXiv:2010.12307*, 2020.
- [14] W. Xia, Y. Yang, J.-H. Xue, and W. Feng, “Controllable continuous gaze redirection,” in *Proceedings of the 28th ACM International Conference on Multimedia*, pp. 1782–1790, 2020.
- [15] I. J. Goodfellow, J. Pouget-Abadie, M. Mirza, B. Xu, D. Warde-Farley, S. Ozair, A. Courville, and Y. Bengio, “Generative adversarial networks,” *arXiv preprint arXiv:1406.2661*, 2014.
- [16] B. Usman, N. Dufour, K. Saenko, and C. Bregler, “Puppetgan: Cross-domain image manipulation by demonstration,” in *2019 IEEE/CVF International Conference on Computer Vision (ICCV)*, pp. 9449–9457, 2019.

- [17] M. Kowalski, S. J. Garbin, V. Estellers, T. Baltrušaitis, M. Johnson, and J. Shotton, “Config: Controllable neural face image generation,” in *European Conference on Computer Vision (ECCV)*, 2020.
- [18] S. Park, S. D. Mello, P. Molchanov, U. Iqbal, O. Hilliges, and J. Kautz, “Few-shot adaptive gaze estimation,” in *Proceedings of the IEEE/CVF International Conference on Computer Vision*, pp. 9368–9377, 2019.
- [19] K. Krafka, A. Khosla, P. Kellnhofer, H. Kannan, S. Bhandarkar, W. Matusik, and A. Torralba, “Eye tracking for everyone,” in *Proceedings of the IEEE conference on computer vision and pattern recognition*, pp. 2176–2184, 2016.
- [20] X. Zhang, Y. Sugano, M. Fritz, and A. Bulling, “Appearance-based gaze estimation in the wild,” in *Proceedings of the IEEE conference on computer vision and pattern recognition*, pp. 4511–4520, 2015.
- [21] B. A. Smith, Q. Yin, S. K. Feiner, and S. K. Nayar, “Gaze locking: passive eye contact detection for human-object interaction,” in *Proceedings of the 26th annual ACM symposium on User interface software and technology*, pp. 271–280, 2013.
- [22] D. Kononenko and V. Lempitsky, “Learning to look up: Realtime monocular gaze correction using machine learning,” in *Proceedings of the IEEE Conference on Computer Vision and Pattern Recognition*, pp. 4667–4675, 2015.
- [23] Y. Ganin, D. Kononenko, D. Sungatullina, and V. Lempitsky, “Deepwarp: Photorealistic image resynthesis for gaze manipulation,” in *European conference on computer vision*, pp. 311–326, Springer, 2016.
- [24] J. Chen, J. Zhang, E. Sangineto, T. Chen, J. Fan, and N. Sebe, “Coarse-to-fine gaze redirection with numerical and pictorial guidance,” in *Proceedings of the IEEE/CVF Winter Conference on Applications of Computer Vision*, pp. 3665–3674, 2021.
- [25] Y. Yu, G. Liu, and J.-M. Odobez, “Improving few-shot user-specific gaze adaptation via gaze redirection synthesis,” in *Proceedings of the IEEE/CVF Conference on Computer Vision and Pattern Recognition*, pp. 11937–11946, 2019.
- [26] Z. He, A. Spurr, X. Zhang, and O. Hilliges, “Photo-realistic monocular gaze redirection using generative adversarial networks,” in *Proceedings of the IEEE/CVF International Conference on Computer Vision*, pp. 6932–6941, 2019.
- [27] E. Wood, T. Baltrušaitis, L.-P. Morency, P. Robinson, and A. Bulling, “Gazedirector: Fully articulated eye gaze redirection in video,” in *Computer Graphics Forum*, vol. 37, pp. 217–225, Wiley Online Library, 2018.
- [28] T. Park, M.-Y. Liu, T.-C. Wang, and J.-Y. Zhu, “Semantic image synthesis with spatially-adaptive normalization,” in *Proceedings of the IEEE/CVF Conference on Computer Vision and Pattern Recognition*, pp. 2337–2346, 2019.
- [29] G. E. Hinton, A. Krizhevsky, and S. D. Wang, “Transforming auto-encoders,” in *International conference on artificial neural networks*, pp. 44–51, Springer, 2011.
- [30] D. E. Worrall, S. J. Garbin, D. Turmukhambetov, and G. J. Brostow, “Interpretable transformations with encoder-decoder networks,” in *Proceedings of the IEEE International Conference on Computer Vision*, pp. 5726–5735, 2017.
- [31] M. Mathieu, J. Zhao, P. Sprechmann, A. Ramesh, and Y. LeCun, “Disentangling factors of variation in deep representations using adversarial training,” *arXiv preprint arXiv:1611.03383*, 2016.
- [32] S. Qian, K.-Y. Lin, W. Wu, Y. Liu, Q. Wang, F. Shen, C. Qian, and R. He, “Make a face: Towards arbitrary high fidelity face manipulation,” in *Proceedings of the IEEE/CVF International Conference on Computer Vision*, pp. 10033–10042, 2019.
- [33] E. Zakharov, A. Shysheya, E. Burkov, and V. Lempitsky, “Few-shot adversarial learning of realistic neural talking head models,” in *Proceedings of the IEEE/CVF International Conference on Computer Vision*, pp. 9459–9468, 2019.
- [34] Y. Choi, M. Choi, M. Kim, J.-W. Ha, S. Kim, and J. Choo, “Stargan: Unified generative adversarial networks for multi-domain image-to-image translation,” in *Proceedings of the IEEE conference on computer vision and pattern recognition*, pp. 8789–8797, 2018.
- [35] I. Higgins, L. Matthey, A. Pal, C. Burgess, X. Glorot, M. Botvinick, S. Mohamed, and A. Lerchner, “beta-vae: Learning basic visual concepts with a constrained variational framework,” 2016.

- [36] X. Chen, Y. Duan, R. Houthoofd, J. Schulman, I. Sutskever, and P. Abbeel, “Infogan: Interpretable representation learning by information maximizing generative adversarial nets,” *arXiv preprint arXiv:1606.03657*, 2016.
- [37] R. T. Chen, X. Li, R. Grosse, and D. Duvenaud, “Isolating sources of disentanglement in variational autoencoders,” *arXiv preprint arXiv:1802.04942*, 2018.
- [38] H.-Y. Lee, H.-Y. Tseng, J.-B. Huang, M. Singh, and M.-H. Yang, “Diverse image-to-image translation via disentangled representations,” in *Proceedings of the European conference on computer vision (ECCV)*, pp. 35–51, 2018.
- [39] X. Huang, M.-Y. Liu, S. Belongie, and J. Kautz, “Multimodal unsupervised image-to-image translation,” in *Proceedings of the European conference on computer vision (ECCV)*, pp. 172–189, 2018.
- [40] Y.-C. Liu, Y.-Y. Yeh, T.-C. Fu, S.-D. Wang, W.-C. Chiu, and Y.-C. F. Wang, “Detach and adapt: Learning cross-domain disentangled deep representation,” in *Proceedings of the IEEE Conference on Computer Vision and Pattern Recognition*, pp. 8867–8876, 2018.
- [41] J. Johnson, A. Alahi, and L. Fei-Fei, “Perceptual losses for real-time style transfer and super-resolution,” in *European conference on computer vision*, pp. 694–711, Springer, 2016.
- [42] K. Simonyan and A. Zisserman, “Very deep convolutional networks for large-scale image recognition,” *arXiv preprint arXiv:1409.1556*, 2014.
- [43] A. Krizhevsky, I. Sutskever, and G. E. Hinton, “Imagenet classification with deep convolutional neural networks,” *Advances in neural information processing systems*, vol. 25, pp. 1097–1105, 2012.
- [44] E. Tzeng, J. Hoffman, K. Saenko, and T. Darrell, “Adversarial discriminative domain adaptation,” in *Proceedings of the IEEE conference on computer vision and pattern recognition*, pp. 7167–7176, 2017.
- [45] X. Zhang, Y. Sugano, M. Fritz, and A. Bulling, “It’s written all over your face: Full-face appearance-based gaze estimation,” in *Proceedings of the IEEE Conference on Computer Vision and Pattern Recognition Workshops*, pp. 51–60, 2017.
- [46] K. He, X. Zhang, S. Ren, and J. Sun, “Deep residual learning for image recognition,” in *Proceedings of the IEEE conference on computer vision and pattern recognition*, pp. 770–778, 2016.
- [47] P. Isola, J.-Y. Zhu, T. Zhou, and A. A. Efros, “Image-to-image translation with conditional adversarial networks,” in *Proceedings of the IEEE conference on computer vision and pattern recognition*, pp. 1125–1134, 2017.
- [48] X. Zhang, Y. Sugano, and A. Bulling, “Revisiting data normalization for appearance-based gaze estimation,” in *Proceedings of the 2018 ACM Symposium on Eye Tracking Research & Applications*, pp. 1–9, 2018.
- [49] M. Heusel, H. Ramsauer, T. Unterthiner, B. Nessler, and S. Hochreiter, “Gans trained by a two time-scale update rule converge to a local nash equilibrium,” *arXiv preprint arXiv:1706.08500*, 2017.
- [50] R. Zhang, P. Isola, A. A. Efros, E. Shechtman, and O. Wang, “The unreasonable effectiveness of deep features as a perceptual metric,” in *Proceedings of the IEEE conference on computer vision and pattern recognition*, pp. 586–595, 2018.
- [51] C. Szegedy, V. Vanhoucke, S. Ioffe, J. Shlens, and Z. Wojna, “Rethinking the inception architecture for computer vision,” in *Proceedings of the IEEE conference on computer vision and pattern recognition*, pp. 2818–2826, 2016.
- [52] A. Krizhevsky, “One weird trick for parallelizing convolutional neural networks,” *arXiv preprint arXiv:1404.5997*, 2014.
- [53] Y. Sugano, Y. Matsushita, and Y. Sato, “Learning-by-synthesis for appearance-based 3d gaze estimation,” in *Proceedings of the IEEE Conference on Computer Vision and Pattern Recognition*, pp. 1821–1828, 2014.
- [54] P. Hu and D. Ramanan, “Finding tiny faces,” in *Proceedings of the IEEE conference on computer vision and pattern recognition*, pp. 951–959, 2017.
- [55] J. Deng, Y. Zhou, S. Cheng, and S. Zaferiou, “Cascade multi-view hourglass model for robust 3d face alignment,” in *2018 13th IEEE International Conference on Automatic Face & Gesture Recognition (FG 2018)*, pp. 399–403, IEEE, 2018.

- [56] P. Huber, G. Hu, R. Tena, P. Mortazavian, P. Koppen, W. J. Christmas, M. Ratsch, and J. Kittler, “A multiresolution 3d morphable face model and fitting framework,” in *Proceedings of the 11th International Joint Conference on Computer Vision, Imaging and Computer Graphics Theory and Applications*, 2016.
- [57] D. P. Kingma and J. Ba, “Adam: A method for stochastic optimization,” *arXiv preprint arXiv:1412.6980*, 2014.
- [58] G. Huang, Z. Liu, L. Van Der Maaten, and K. Q. Weinberger, “Densely connected convolutional networks,” in *Proceedings of the IEEE conference on computer vision and pattern recognition*, pp. 4700–4708, 2017.
- [59] D. Ulyanov, A. Vedaldi, and V. Lempitsky, “Instance normalization: The missing ingredient for fast stylization,” *arXiv preprint arXiv:1607.08022*, 2016.
- [60] S. Ioffe and C. Szegedy, “Batch normalization: Accelerating deep network training by reducing internal covariate shift,” in *International conference on machine learning*, pp. 448–456, PMLR, 2015.
- [61] J. Deng, W. Dong, R. Socher, L.-J. Li, K. Li, and L. Fei-Fei, “Imagenet: A large-scale hierarchical image database,” in *2009 IEEE conference on computer vision and pattern recognition*, pp. 248–255, Ieee, 2009.

## A Implementation details

In this section, we provide an overview of the data pre-processing pipeline followed by training and architectural details of CUDA-GR.

### A.1 Data Pre-processing

We follow the same data pre-processing pipeline as done in [18]. The pipeline consists of a normalization technique [48] initially introduced by [53]. It is followed by face detection [54] and facial landmarks detection [55] modules for which open-source implementations are publicly available. The Surrey Face Model [56] is used as a reference 3D face model. Further details can be found in [18]. To summarize, we use the public code<sup>4</sup> provided by Park et al. [18] to produce image patches of size  $64 \times 256$  containing both eyes.

### A.2 Training Details

**Hyperparameters** For both GazeCapture  $\rightarrow$  MPIIGaze and GazeCapture  $\rightarrow$  Columbia training, we use a batch size of 8, and training is done for 200k iterations. We use Adam optimizer [57] for all network modules with a weight decay coefficient of  $10^{-4}$  and the rest of the parameters have default values. The initial learning rate is 0.0004 and is decayed by a factor of 0.8 after approximately 34k iterations. The weights of the objective function are set as  $\lambda_R = 200$ ,  $\lambda_P = 0.0001$ ,  $\lambda_C = 0.1$ ,  $\lambda_G = 1$  and  $\lambda_F = 1$ .

**Data Split** In GazeCapture [19] dataset, we use the training subset from the data split provided by [19] and is chosen as source domain labeled data. In the GazeCapture  $\rightarrow$  MPIIGaze setting, we select the first 11 user’s data of MPIIGaze [45] for training, and for GazeCapture  $\rightarrow$  Columbia training, we use the first 50 participant’s data from Columbia [21], both of which forms the target domain dataset. We evaluate our model on the entire MPIIGaze and Columbia dataset. Note that, we do not use any labels from the target domain dataset during training.

### A.3 Architecture Details

In this section, we provide architectural details of our network CUDA-GR and task network  $\mathcal{T}$ .

#### A.3.1 Our framework CUDA-GR

We use DenseNet architecture [58] to implement both image encoders ( $\mathbf{E}_S$  and  $\mathbf{E}_T$ ) and a generator ( $\mathbf{G}$ ). The DenseNet is formed with a growth rate of 32, 4 dense blocks (each with 4 composite layers), and a compression factor of 1.0. We use instance normalization [59] and leaky ReLU activation functions ( $\alpha = 0.01$ ) for all the layers in the network. We remove dropout and  $1 \times 1$  convolution layers. The dimensions of latent factors  $z^a$ ,  $z^g$ , and  $z^h$  are set to be equal to 16, 8, and 16 respectively. Thus, to project CNN features to the latent features, we use global-average pooling and pass through a fully-connected layer to output feature of dimension 16 for  $\mathbf{E}_S$ , and 40 for  $\mathbf{E}_T$ . For the generator network, we use de-convolution layers (of stride 1) instead of convolutions and replace average-pooling layers with  $3 \times 3$  de-convolution layers. Before passing through the generator, we apply a fully-connected layer to project the latent features back to the CNN features with a shape of 2 feature maps, width 8 and height 2.

The gaze encoder  $\mathbf{F}_g$  and head pose encoder  $\mathbf{F}_h$  are MLP-based blocks whose architecture is shown in Table 3. The input dimensions for both these networks is 2 and output dimensions are equal to  $z^g$  ( $= 8$ ) and  $z^h$  ( $= 16$ ) for  $\mathbf{F}_g$  and  $\mathbf{F}_h$  respectively.

The latent domain discriminator network  $\mathbf{D}_F$  consists of 4 MLP layers as shown in Table 4. It takes the input of dimension 40 and gives 1-dimensional output.

Both image discriminators  $\mathbf{D}_T$  and  $\mathbf{D}_S$  are PatchGAN [47] based networks as used in [13]. The architecture of the discriminator is described in Table 5.

The task network  $\mathcal{T}$  is a ResNet-50 [46] model with batch normalization [60] replaced by instance normalization [59] layers. The input to this network is of size  $64 \times 256$  and gives a 4-dimensional

<sup>4</sup>[https://github.com/swook/faze\\_preprocess](https://github.com/swook/faze_preprocess)

output describing pitch and yaw angles for both gaze and head directions. It is initialized with ImageNet [61] pre-trained weights and is fine-tuned on the GazeCapture training subset for around 190k iterations. The GazeCapture validation subset is used to select the best performing model. The initial learning rate is 0.0016 which is decayed by a factor of 0.8 after about 34k iterations and is trained using Adam [57] optimizer with a weight decay coefficient of  $10^{-4}$ . The architecture of  $\mathcal{T}$  is summarized in Table 6.

Table 3: Architecture of the gaze  $\mathbf{F}_g$  and head pose  $\mathbf{F}_h$  encoders. We choose  $o_{dim} = 8$  for  $\mathbf{F}_g$ , and  $o_{dim} = 16$  for  $\mathbf{F}_h$ .

Layer name	Activation	Output shape
Fully connected	LeakyReLU ( $\alpha = 0.01$ )	2
Fully connected	LeakyReLU ( $\alpha = 0.01$ )	2
Fully connected	LeakyReLU ( $\alpha = 0.01$ )	2
Fully connected	None	$o_{dim}$

Table 4: Architecture of the latent domain discriminator  $\mathbf{D}_F$ .

Layer name	Activation	Output shape
Fully connected	LeakyReLU ( $\alpha = 0.01$ )	40
Fully connected	LeakyReLU ( $\alpha = 0.01$ )	40
Fully connected	LeakyReLU ( $\alpha = 0.01$ )	40
Fully connected	None	1

Table 5: Architecture of the image discriminator networks  $\mathbf{D}_T$  and  $\mathbf{D}_S$ . Note that, both the discriminators has the same architecture.

Layer name	Kernel, Stride, Padding	Activation	Normalization	Output shape
Conv2d	$4 \times 4, 2, 1$	LeakyReLU ( $\alpha = 0.2$ )	-	$64 \times 32 \times 128$
Conv2d	$4 \times 4, 2, 1$	LeakyReLU ( $\alpha = 0.2$ )	InstanceNorm	$128 \times 16 \times 64$
Conv2d	$4 \times 4, 2, 1$	LeakyReLU ( $\alpha = 0.2$ )	InstanceNorm	$256 \times 8 \times 32$
Conv2d	$4 \times 4, 1, 1$	LeakyReLU ( $\alpha = 0.2$ )	InstanceNorm	$512 \times 7 \times 31$
Conv2d	$4 \times 4, 1, 1$	-	-	$1 \times 6 \times 30$

### A.3.2 Gaze Estimation Model

We train a ResNet-50 model similar to the architecture of  $\mathcal{T}$  (as shown in Table 6) for the downstream gaze estimation task. Both cross-dataset and cross-subject models are trained with a batch size of 16 and a fixed learning rate of 0.001. We used Adam optimizer with a weight decay coefficient of  $10^{-4}$ . The number of iterations used to train the cross-dataset model is 50k while for the cross-subject model is 20k. We randomly sample one user data to validate the cross-subject model.

### A.3.3 State-of-the-art Baselines

We re-implement the ST-ED [13] for a fair comparison with our method. Here are the details for the reimplementation.

**Self Transforming Encoder Decoder (ST-ED)** ST-ED is originally implemented on full face images of size  $128 \times 128$ . We train this model on the images containing both eyes (size  $64 \times 256$ ) to ensure a fair comparison using the public code<sup>5</sup> available and use the same hyperparameters as provided by the original implementation. For the faithful comparison, we replaced *tanh* non-linearity with an identity function and removed a constant factor of  $0.5\pi$  in all the modules.

<sup>5</sup><https://github.com/zhengyuf/STED-gaze>



Table 6: Architecture of the task network  $\mathcal{T}$ .

Module/Layer name	Output shape
ResNet-50 layers with MaxPool stride=1	$2048 \times 1 \times 1$
Fully connected	4

## B More details on Consistency Loss

Here we provide details for the head consistency loss defined in Equation 13. Similar to the gaze consistency loss, it constitutes two terms: *label consistency loss* and *redirection consistency loss*. The first term *label consistency loss* ensures the consistency in head pose labels of the generated image  $\hat{X}_{\{T,S\}}$  and the input image  $X_{\{T,S\}}$ , while the second term *redirection consistency loss* maintains the pseudo-labels for the head redirected images, i.e.,  $\mathcal{T}^h(\hat{X}_T^g) = \mathcal{T}^h(X_T)$  and  $\mathcal{T}^h(\hat{X}_T^h) = \mathcal{T}^h(X_S)$ , where  $\hat{X}_T^h = \mathbf{G}(z_T^a \oplus z_T^g \oplus z_S^h)$ .

$$\begin{aligned} \mathcal{L}_{head} = & \underbrace{\mathcal{L}_{ang}(\mathcal{T}^h(\hat{X}_S), \mathcal{T}^h(X_S)) + \mathcal{L}_{ang}(\mathcal{T}^h(\hat{X}_T), \mathcal{T}^h(X_T))}_{\text{label consistency loss}} \\ & + \underbrace{\mathcal{L}_{ang}(\mathcal{T}^h(\hat{X}_T^g), \mathcal{T}^h(X_T)) + \mathcal{L}_{ang}(\mathcal{T}^h(\hat{X}_T^h), \mathcal{T}^h(X_S))}_{\text{redirection consistency loss}} \end{aligned} \quad (13)$$

## C Ablation Study on Loss Terms

In Table 7, we compare against the ablations of our full loss terms. As can be seen, each loss term is critical for the improvement in performance. We see a substantial improvement in LPIPS with the addition of  $\mathcal{L}_{feat}$ . The ablation study is done for GazeCapture  $\rightarrow$  MPIIGaze setting.

Table 7: **Ablation Study:** Following table shows the ablations of the various loss terms on GazeCapture  $\rightarrow$  MPIIGaze experiment. As can be seen, we see an improvement in the performance with the addition of each loss term.

GazeCapture $\rightarrow$ MPIIGaze	
Loss	LPIPS $\downarrow$
$\mathcal{L}_{recon} + \mathcal{L}_{gen}$	0.424
$+ \mathcal{L}_{perc}$	0.378
$+ \mathcal{L}_{consistency}$	0.357
$+ \mathcal{L}_{feat}$	<b>0.266</b>

## D Additional Results

In Figure 6, we show additional qualitative results for both target datasets, MPIIGaze (Figure 6 (a)) and Columbia (Figure 6 (b)). We compare our method CUDA-GR against the state-of-the-art baselines.

Figure 6: **Additional Qualitative Results:** Our method CUDA-GR generates better quality and photo-realistic images as compared to the baseline methods FAZE [18] and ST-ED [13]. The first column shows the gaze source images from which gaze information is used to redirect. The second column shows the input images from the target domain data. Best viewed in color.



(a) Qualitative results on MPIIGaze dataset (GazeCapture  $\rightarrow$  MPIIGaze)



(b) Qualitative results on Columbia dataset (GazeCapture  $\rightarrow$  Columbia)

### D.1 Failure Cases

Figure 7 shows some failure cases where our method demonstrates difficulties in faithfully redirecting the head pose of the input image (Column 2) in the direction same as that of the source image (Column 1).

Figure 7: **Failure cases:** Our method shows difficulties in manipulating the head pose of the input images (Column 2) to the direction of the source images (Column 1).

